



RESEARCH LETTER

10.1029/2017GL076862

Key Points:

- Reconnection simulations produce intense energy conversion that exceeds expectations and resembles spacecraft observations
- Unlike in symmetric reconnection, the dissipation is driven by the annihilation of the out-of-plane (Hall) magnetic field
- Electron dynamics explain the localized and spatially oscillatory features

Correspondence to:

M. Swisdak,
swisdak@umd.edu

Citation:

Swisdak, M., Drake, J. F., Price, L., Burch, J. L., Cassak, P. A., & Phan, T.-D. (2018). Localized and intense energy conversion in the diffusion region of asymmetric magnetic reconnection. *Geophysical Research Letters*, 45, 5260–5267. <https://doi.org/10.1029/2017GL076862>



Received 18 DEC 2017

Accepted 11 MAY 2018

Accepted article online 16 MAY 2018

Published online 5 JUN 2018

Localized and Intense Energy Conversion in the Diffusion Region of Asymmetric Magnetic Reconnection

M. Swisdak¹ , J. F. Drake¹ , L. Price¹ , J. L. Burch² , P. A. Cassak³ , and T.-D. Phan⁴ 

¹IREAP, University of Maryland, College Park, MD, USA, ²Southwest Research Institute, San Antonio, TX, USA, ³Department of Physics and Astronomy, West Virginia University, Morgantown, WV, USA, ⁴Space Sciences Laboratory, University of California, Berkeley, CA, USA

Abstract We analyze a high-resolution simulation of magnetopause reconnection observed by the Magnetospheric Multiscale mission and explain the occurrence of strongly localized dissipation with an amplitude more than an order of magnitude larger than expected. Unlike symmetric reconnection, wherein reconnection of the ambient reversed magnetic field drives the dissipation, we find that the annihilation of the self-generated, out-of-plane (Hall) magnetic field plays the dominant role. Electrons flow along the magnetosheath separatrices, converge in the diffusion region, and jet past the X-point into the magnetosphere. The resulting accumulation of negative charge generates intense parallel electric fields that eject electrons along the magnetospheric separatrices and produce field-aligned beams. Many of these features match Magnetospheric Multiscale observations.

Plain Language Summary The Magnetospheric Multiscale mission is designed to observe magnetic reconnection, a process where the energy in magnetic fields is transferred to the surrounding particles. Recent observations by Magnetospheric Multiscale have shown that this transfer is patchy and much stronger than anticipated. This paper presents computer simulations explaining why this might be the case.

1. Introduction

Magnetic reconnection transfers energy from the magnetic field to the surrounding plasma. Oppositely directed components of the field undergo topological reordering at X-points, which form within electron diffusion regions where the magnetic field is no longer frozen into any component of the plasma. In the simplest (symmetric) case the two plasmas upstream from an X-point differ only in the orientation of the embedded magnetic field and the electron diffusion region is elongated along the outflow direction but otherwise relatively unstructured (Shay et al., 2007).

However, reconnection also occurs in asymmetric configurations in which the abutting plasmas differ in density, temperature, and magnetic field strength (Cassak & Shay, 2007; Sonnerup et al., 1981), for example, Earth's magnetopause, the boundary separating the hot and tenuous plasma of the magnetosphere from the magnetosheath and its shocked plasma of solar wind origin. The structure of asymmetric reconnection, and magnetopause reconnection in particular, has remained unclear, with some arguing that a localized electron diffusion region does not develop, even in the special case where the opposing fields are antiparallel (Mozer & Pritchett, 2009; Pritchett & Mozer, 2009).

Recent observations by the Magnetospheric Multiscale (MMS) mission have triggered new interest in the structure of the electron diffusion region during asymmetric reconnection. Crescent-shaped electron velocity-space distributions that had been predicted by simulations (Hesse et al., 2014) were seen (Burch et al., 2016; Chen et al., 2016), and the role of the large normal electric field, which points sunward across the magnetopause and balances the ambient ion pressure gradient, in driving the crescents to higher energies was established (Bessho et al., 2016; Chen et al., 2016; Egedal et al., 2016; Shay et al., 2016). In contradiction to earlier models and observations, the data suggest that energy conversion within the electron diffusion region is associated with oblique whistler-like disturbances featuring intense parallel electric fields and oscillations in $\mathbf{J} \cdot \mathbf{E}$ of unknown origin. The local dissipation rate is nearly 2 orders of magnitude greater than expected (Burch et al., 2018).

Here we use a high-resolution particle-in-cell (PIC) simulation to explore the structure of asymmetric reconnection in a system with initial conditions based on MMS observations (Burch et al., 2016, 2018). We demonstrate that a jet of electrons streaming toward the magnetosphere and across the X-point produces a standing structure with nonuniform but intense energy conversion (such structures can also be seen, although are not explained, in Cassak et al., 2017). Unlike in symmetric reconnection, the energy transfer arises from the annihilation of the Hall (out-of-plane) component of the magnetic field. The most significant annihilation does not occur at the X-point but instead is shifted toward the magnetosphere and the fluid stagnation point. The electrons are ejected from the diffusion region by intense parallel electric fields and not, as in the symmetric case, by the reconnected magnetic field. The simulation reproduces the key features of the observations.

2. Simulations

We perform the simulations with the PIC code `p3d` (Zeiler et al., 2002). In its normalization a reference magnetic field strength B_0 and density n_0 define the velocity unit $v_{A0} = B_0 / \sqrt{4\pi m_i n_0}$. Times are normalized to the inverse ion cyclotron frequency $\Omega_{i0}^{-1} = m_i c / e B_0$, lengths to the ion inertial length $d_{i0} = c / \omega_{pi0}$ (where $\omega_{pi0} = \sqrt{4\pi n_0 e^2 / m_i}$ is the ion plasma frequency), electric fields to $v_{A0} B_0 / c$, and temperatures to $m_i v_{A0}^2$. In the system considered here B_0 and n_0 correspond to their asymptotic magnetosheath values: $B_0 = 23$ nT and $n_0 = 11.3$ cm⁻³.

The initial conditions closely mimic those observed during the diffusion region encounter described in Burch et al. (2016). We employ an *LMN* coordinate system in which the reconnecting field parallels the *L* axis (roughly north-south), the *M* axis runs roughly east-west, with dawnward positive, and the *N* axis points radially away from Earth and completes the right-handed triad. The reconnecting component of the field B_L and the ion and electron temperatures, T_i and T_e , vary as functions of *N* with hyperbolic tangent profiles of width 1. The asymptotic values of n , B_L , T_i , and T_e in code units are 1.0, 1.0, 1.37, and 0.12 in the magnetosheath and 0.06, 1.70, 7.73, and 1.28 in the magnetosphere. Pressure balance determines the initial density profile. The guide field $B_M = 0.099$ is much smaller than B_L (i.e., the reconnection is nearly antiparallel) and initially uniform. While not an exact kinetic equilibrium, the unperturbed configuration is in force balance and would not undergo significant evolution during the timescales considered here. We impose a small initial perturbation in order to trigger reconnection at a single and specific point.

The ion-to-electron mass ratio is chosen to be 100, which is sufficient to separate the electron and ion scales (the electron inertial length $d_{e0} = 0.1 d_{i0}$). The normalized speed of light is $c = 15$ so that $\omega_{pe} / \Omega_{ce} = 1.5$ in the asymptotic magnetosheath and ≈ 0.2 in the asymptotic magnetosphere; the observed ratios are larger, ≈ 46 and 7, and as a consequence the simulation's Debye length is larger than in the real system. However, since the development of reconnection does not appreciably depend on physical effects at the Debye scale, the expected impact is minimal. The spatial grid has resolution $\Delta = 0.01$ in normalized units, while the Debye length in the simulation's magnetosheath, ≈ 0.03 , is the smallest physical scale. To ameliorate numerical noise, particularly in the low-density magnetosphere, each grid cell initially contains 3,000 weighted macroparticles, substantially more than typical PIC simulations.

The computational domain of the principal simulation discussed here has dimensions $(L_L, L_N) = (40.96, 20.48)$ with periodic boundary conditions used in all directions. While particles can move in the *M* direction, variations in physical quantities are not permitted, $\partial / \partial M = 0$. This simplification greatly eases the computational burden while still allowing reconnection to proceed. We also compare some of our results with those from a fully three-dimensional simulation of the same event previously described in Price et al. (2016).

3. Results

We first discuss the case of symmetric reconnection in order to provide background for the significantly larger energy conversion rates seen in the observations and the simulations. Direct manipulation of Maxwell's equations gives Poynting's theorem:

$$\frac{\partial U}{\partial t} + \frac{c}{4\pi} \nabla \cdot (\mathbf{E} \times \mathbf{B}) = -\mathbf{J} \cdot \mathbf{E}, \quad (1)$$

where $U = (E^2 + B^2) / 8\pi$ is the electromagnetic energy density, the second term defines the Poynting flux $\mathbf{S} = c(\mathbf{E} \times \mathbf{B}) / 4\pi$, and $\mathbf{J} \cdot \mathbf{E}$ quantifies the rate of energy transfer, being positive when directed from the fields

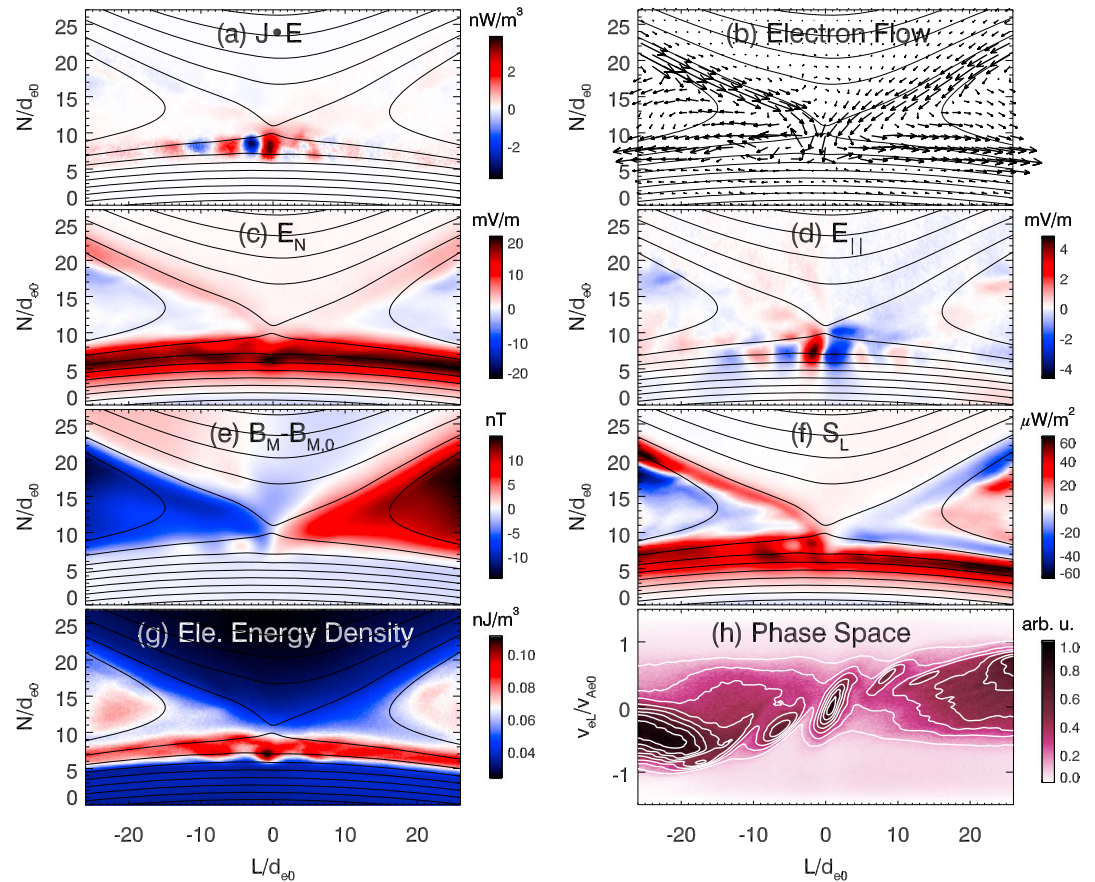


Figure 1. Simulation results from a region centered on the X-point. (a) The $\mathbf{J} \cdot \mathbf{E}$ term from Poynting's theorem. (b) In-plane electron flow field. (c) E_N , the normal component of the electric field. (d) E_{\parallel} , the component of the electric field parallel to the magnetic field. (e) $B_M - B_{M,0}$, the change in the out-of-plane component of the magnetic field from its (spatially constant) initial value. (f) S_L , the horizontal component of the Poynting flux. (g) Electron energy density. (h) $v_L - L$ electron phase space overlaid with contours. Magnetic field lines have been overplotted in panels (a)–(g). Distances are normalized to the electron inertial length $d_{e0} = d_{i0} \sqrt{m_e/m_i} = 0.1d_{i0}$.

to the particles. During symmetric reconnection the M component of the electric field drives an elongated (in the L direction) layer of electron current density J_M . The product $J_M E_M$ matches the divergence of the incoming Poynting flux associated with the reconnecting field ($\sim E_M B_L$). However, this scaling cannot explain MMS measurements of magnetopause reconnection. For reasonable parameters—current density $J_M \sim 1 \mu\text{A}/\text{m}^2$ and reconnection electric field $E_M \sim 0.2 \text{ mV}/\text{m}$ —the resulting $J_M E_M \sim 0.2 \text{ nW}/\text{m}^3$ greatly underestimates the observations, which can exceed $10 \text{ nW}/\text{m}^3$ (Burch et al., 2016; Ergun et al., 2016; Eriksson et al., 2016). Hence, the energy conversion processes that dominate during symmetric reconnection likely do not play a significant role at the magnetopause.

We now show that high-resolution simulations of asymmetric reconnection can produce large rates of energy conversion and discuss the underlying physical mechanism. Figure 1 gives an overview of the simulation at $t = 32\Omega_i^{-1}$, a time of steady state reconnection. The magnetosheath lies at the top of each panel and the magnetosphere at the bottom (equivalently, earthward is down), while the horizontal axis roughly points north-south because the MMS encounter occurred near the equatorial plane. The reconnecting component of the field is in the $+L$ direction in the magnetosphere and the $-L$ direction in the magnetosheath; representative field lines are overplotted in panels (a)–(g). The color bar labels have been converted from the simulation's normalization to meter-kilogram-second units.

Panel (a) shows the structure of $\mathbf{J} \cdot \mathbf{E}$. Strikingly, regions of positive (red) and negative (blue) signs coexist, the latter representing a transfer of energy from the plasma to the fields, the opposite of the usual behavior during reconnection. The rate of energy conversion in the electron frame (Zenitani et al., 2011), $\mathbf{J} \cdot \mathbf{E}' = \mathbf{J} \cdot (\mathbf{E} + \mathbf{v}_e \times \mathbf{B}/c)$, is essentially identical because the electron contribution dominates the current density (Cassak et al., 2017).

Although the X-point slowly drifts in the L direction during the simulation, the structure of $\mathbf{J} \cdot \mathbf{E}$ undergoes minimal temporal evolution and remains stationary in the X-point frame.

Unlike in symmetric reconnection, the primary contribution to the dissipation comes from $J_N E_N$. High-density magnetosheath plasma flows in the N direction across the X-point and into the low-density magnetosphere. (As is generally the case in asymmetric reconnection, the magnetic X-point and the flow stagnation point do not coincide (Cassak & Shay, 2007).) The $v_N B_L$ Lorentz force redirects the motion of both the electrons and the ions, but the larger masses of the latter let them penetrate farther into the magnetosphere. The resulting charge imbalance produces a large E_N that retards the ion motion and balances the ion pressure gradient (Pritchett, 2008) while also accelerating electrons toward the magnetosphere. Panel (b) shows the electron flow and, in particular, the N directed flow across the X-point. Panel (c) shows the strong positive magnetospheric E_N that results from the separation of positive and negative charge. This separation occurs along the entire magnetospheric separatrix due to the different spatial scales associated with electrons and ions.

The interaction of the current due to the electron flow with E_N produces the large region of positive $\mathbf{J} \cdot \mathbf{E}$ near the center of panel (a). Since $J_N \sim J_M$ in the simulation, it is the large value of $E_N \sim 20$ mV/m $\gg E_M$ that makes the most significant contribution to the energy transfer rate and causes the local dissipation rate to greatly exceed expected values. We return to the energy source of this intense dissipation after completing the discussion of the diffusion region geometry.

Many of the electrons that cross the X-point first accelerate along the magnetosheath separatrices, producing the strong flows seen in panel (b). At the stagnation point their excess density leads to the converging bipolar signature in the parallel component of the electric field E_{\parallel} , panel (d), that brackets the region of positive $\mathbf{J} \cdot \mathbf{E}$. This electric field ejects the electrons downstream, producing the flows along the magnetospheric separatrices. As part of the J_M current density that establishes the reversal in B_L , these same streaming electrons have velocity components satisfying $v_M < 0$. Hence, they experience a $v_M B_L$ Lorentz force that pushes them in the positive N direction. Since B_L decreases when moving toward the magnetopause, E_N is eventually strong enough to counteract the Lorentz force and again direct the electrons toward the magnetosphere. While continuing downstream, they execute sinusoidal oscillations (with decaying amplitude) in the N direction, each bounce accompanied by a perturbation in the net charge density and corresponding signatures in E_N and E_{\parallel} . (In Figure 1 the effect is strongest on the left side of the X-point; note the motions beginning at $L \approx -5$, $N \approx 8$ in panel [b]. The asymmetry is likely due to the X-point's slow diamagnetic drift; Swisdak et al., 2003, 2010.) Due to these undulations, everywhere $v_N > 0$ the electrons return energy to the fields and produce regions with $\mathbf{J} \cdot \mathbf{E} < 0$. The ejection of electrons downstream from the X-point by $E_L \sim E_{\parallel}$ contrasts sharply with the situation in symmetric reconnection, where it is the normal magnetic field B_N that rotates the out-of-plane streaming electrons (with large v_M) into the outflow direction.

The currents due to the electron flows also produce the large jumps across the separatrices in the out-of-plane component of the magnetic field B_M shown in panel (e). In symmetric reconnection B_M is quadrupolar because the electron flow is inward (toward the X-point) along all four separatrices. The bipolar signature in the asymmetric case arises due to the broken symmetry (Karimabadi et al., 1999; Tanaka et al., 2008), and the resultant high-speed electron flows across the X-point. Most important for the energy conversion shown in Figure 1a is the narrow (in L) jet of electrons with $v_N < 0$ that produces the local reversal in B_M . While this simulation includes a small initial B_M , it has little effect on the system's development other than mildly breaking the symmetry across $L = 0$. A separate simulation with no initial B_M (not shown) exhibits similar features.

To establish the dominant source of the high rate of energy dissipation, we show S_L , the L component of the Poynting flux, in panel (f). Its reversal across the line $L = 0$ gives the dominant contribution to $\nabla \cdot \mathbf{S}$ (and, equivalently, to $\mathbf{J} \cdot \mathbf{E}$). Although not shown here, plots of $\nabla \cdot \mathbf{S}$ and $\mathbf{J} \cdot \mathbf{E}$ exhibit close agreement, supporting the claim that the system is largely in a steady state (see equation (1)). Since $S_L \sim E_N B_M$, it is the annihilation of B_M between the X-point and stagnation point that drives the large energy conversion shown in Figure 1a. Panel (g) shows the electron energy density, $\rho v_e^2/2 + 3nT_e/2$, which peaks at the location of maximum dissipation. The high-energy content that stretches along the magnetospheric separatrix includes a contribution from the local electron current supporting the magnetic field reversal as well as from the transport of energy from the dissipation region near the X-point.

We conclude that in asymmetric reconnection the formation of a large Hall magnetic field B_M and its associated dissipation is the dominant driver of magnetic energy release in the electron diffusion region.

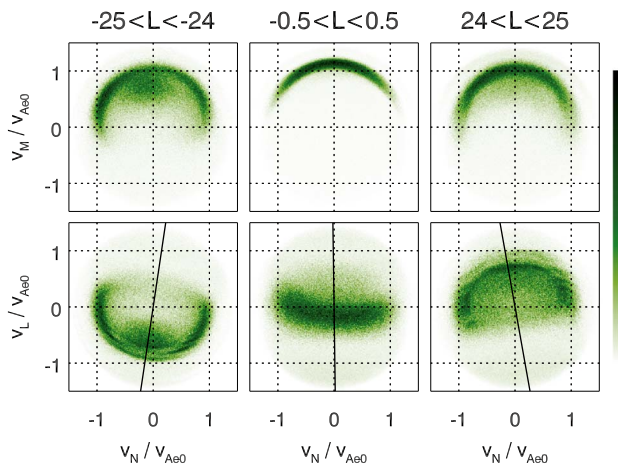


Figure 2. Two-dimensional electron velocity distributions collected at $7 < N < 8$ and the far left, center, and far right of the domain shown in Figure 1. The solid lines in the bottom panels indicate the local projection of the magnetic field direction.

ized to the electron Alfvén speed, and, as expected, most of the plasma has been accelerated to $\approx v_{Ae0}$ within a few d_{e0} downstream of the stagnation point/X-point. (The faint background corresponds to hot, tenuous magnetospheric electrons. Most of the particles are colder, denser magnetosheath electrons that have passed through the X- and stagnation points.) The primary central vortex and the secondary adjoining vortices correspond to the oscillations in $\mathbf{J} \cdot \mathbf{E}$. The hot, nearly featureless beams downstream from the stagnation region suggest that the electrons have undergone irreversible heating. In contrast, the ions do not undergo significant heating while traversing this region and the analogous ion phase space (not shown) does not include any fine-scale features.

The features of the electron diffusion region shown in Figure 1 are accompanied by signatures in the electron velocity-space distributions. Figure 2 shows two-dimensional distributions at three locations. Each includes particles found in the range $7 < N < 8$, while the three columns correspond to different locations in L : $-25 < L < -24$, $-0.5 < L < 0.5$, and $24 < L < 25$.

Cusped motions of the electrons in the fields shown in Figure 1 produce crescent distributions in electron velocity space. (As in Figure 1h, hot magnetospheric electrons comprise a faint background population.) The top row shows the distributions in $v_N - v_M$ space with the central panel capturing electrons that have just entered the magnetosphere. The crescents are the perpendicular velocity-space features—the local magnetic field is nearly perpendicular to the M - N plane—predicted from simulations (Hesse et al., 2014) and subsequently observed by MMS (Burch et al., 2016). (While not strictly field aligned, the LMN axes are good proxies for such a coordinate system since the local field points primarily in the L direction.) They arise from magnetosheath electrons streaming across the X-point that have their motion deflected into the positive- M direction where they form the current density J_M that supports the rotation in the reconnecting magnetic field B_L . The bottom row shows the distribution in $v_L - v_N$ space with the solid lines giving the projected orientation of the local magnetic field. The crescents visible in the left and right panels, so-called parallel crescents because of their alignment with the field, have been documented in MMS observations (Burch et al., 2016) and are the result of the electrons that form the central crescents of the top row being accelerated into the L direction by the electric field $E_L \approx E_{\parallel}$ (Shay et al., 2016).

4. Discussion

Although our simulations necessarily include some simplifying approximations, they agree with many features of the MMS observations (Burch et al., 2018) while simultaneously providing a synoptic view. During asymmetric reconnection with a small guide field, we observe spatially oscillatory dissipation signatures in which $\mathbf{J} \cdot \mathbf{E}$ changes sign over a characteristic scale length of a few d_{e0} . These features, observed by MMS but previously unexplained, are a consequence of the electron dynamics. Furthermore, like MMS, we observe both

This dissipation does not peak at the X-point but rather earthward of it in the direction of the stagnation point. We emphasize that the dissipation of B_M does not correspond to reconnection of B_M , which would take place in the L - M plane and therefore is not accessible in the geometry of this simulation. In the companion three-dimensional simulation the region around $L = 0$ in the L - M plane exhibits fluctuations, but there are no organized flows that would indicate the reconnection of the B_M component. This is likely because the width of the current layer $J_N(L)$ supporting the reversal in B_M is $\lesssim 2d_i$ in the N direction and the transit time of current-carrying electrons along the layer is of order Ω_{ci}^{-1} .

Definitively proving the existence of irreversible dissipation in collisionless PIC simulations is not straightforward—merely showing that regions where $\mathbf{J} \cdot \mathbf{E} > 0$ exist is insufficient since reversible processes can generate such signals. The governing Vlasov equation is, in principle, time reversible, but it can also lead to the development of arbitrarily complex structures in phase space. As the complexity increases, weaker and weaker nonideal processes are sufficient to cause irreversible heating and dissipation. Panel (h) shows the electron $v_L - L$ phase space for the domain $N \in (7, 8)$, which intersects the most significant regions of $\mathbf{J} \cdot \mathbf{E}$. The vertical scale is normal-

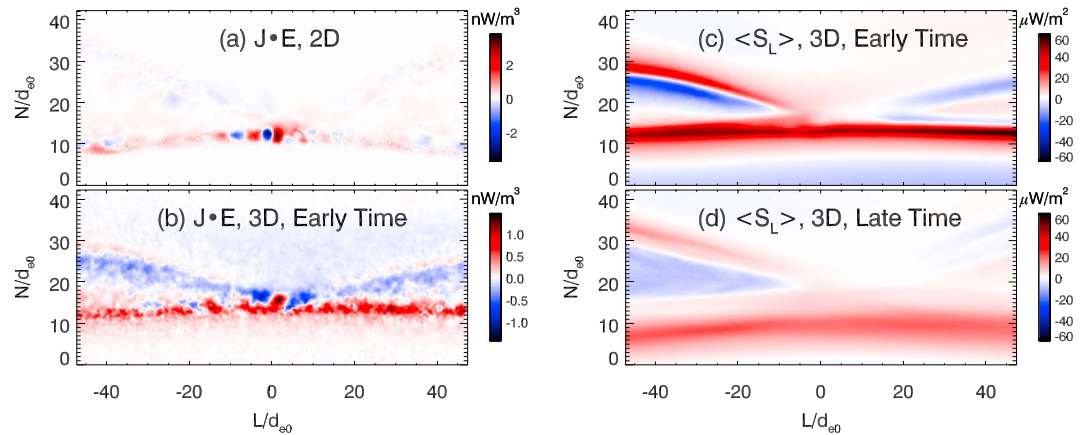


Figure 3. Dissipation and Poynting flux from two-dimensional and three-dimensional simulations. (a) $\mathbf{J} \cdot \mathbf{E}$ from the same high-resolution 2-D simulation shown in Figure 1a. (b) A two-dimensional slice of $\mathbf{J} \cdot \mathbf{E}$ at an early time in the simulation and averaged over $\approx 3d_e$ in the M direction to reduce noise, from the lower-resolution 3-D simulation presented in Price et al. (2016). (c) The average of S_L over the entire M domain from the same time as panel (b). (d) $\langle S_L \rangle$ from later in the same simulation. The panels have been horizontally shifted to align the X-points.

field-aligned beams along the separatrices and phase-space crescents with varying orientations with respect to the local magnetic field, suggesting that the essential physics of the electron flows have been captured.

Nevertheless, discrepancies between the simulations and observations do exist. The oscillations are spatially stationary in the frame of the X-point, include minimal contributions from the ions (i.e., exist in a regime similar to electron-magnetohydrodynamic but where kinetics play a role; Shay & Drake, 1998), and exhibit strongly nonlinear amplitudes. The latter are ≈ 3 – 4 times smaller in the simulations than in the MMS observations, likely as a consequence of the nonphysical mass ratio. The magnitude of E_N is controlled by the ions and hence is insensitive to m_i/m_e , but $J_N \sim B_M/\delta_L$ depends on the electron scale length δ_L . For a realistic m_i/m_e the magnitude of $\mathbf{J} \cdot \mathbf{E}$ should increase by $\approx \sqrt{1,836/100} \approx 4$. Also, although we argue that the oscillations in $\mathbf{J} \cdot \mathbf{E}$ arise from changes in the sign of v_{eN} , no such variations are observed in the MMS data. However, v_{eN} is typically much smaller than either v_{eM} or v_{eL} near X-points, which makes its measurement susceptible to errors arising from small variations in the determination of the LMN coordinate system. Denton et al. (2018) have shown that variations up to 25° are possible, which is more than sufficient to explain the discrepancy.

Three-dimensional simulations of the same event (Le et al., 2017; Price et al., 2016, 2017) have been previously reported. While the two- and three-dimensional systems generate similar large-scale features, two factors lead us to focus on the former. First, because of the reduced dimensionality it is possible to track a substantially larger number of macroparticles (in this case 10^2 – 10^3 times more per typical length scale), which significantly reduces statistical noise. Second, while regions of intense dissipation associated with the annihilation of the Hall magnetic field are seen in each case, the three-dimensional simulation develops structure in the M direction associated with the lower-hybrid drift instability (LHDI) that complicates the analysis of the dissipation mechanism but does not appear to alter the underlying physics.

Figure 3a shows $\mathbf{J} \cdot \mathbf{E}$ in the region surrounding the X-point for the two-dimensional simulation over a slightly larger region than that shown in Figure 1a. Panels (b) and (c) show cuts from the three-dimensional simulation of Price et al. (2016). To reduce the random noise, both panels have been averaged over $\approx 3d_e$ in the M direction; averages over significantly greater distances smear out significant features. Panel (b) comes from early in the simulation before the development of lower-hybrid turbulence. A comparison with panel (a) shows that both the two- and three-dimensional simulations develop analogous features, particularly oscillations in the sign of $\mathbf{J} \cdot \mathbf{E}$ aligned in the L direction and parallel to the magnetospheric separatrix. In addition, the three-dimensional simulation, unlike its two-dimensional counterpart, has a significant signal along the magnetosheath separatrix. The source of this feature is unclear. Spacecraft on trajectories cutting through the outflow in the N direction would also observe an oscillation in the sign of $\mathbf{J} \cdot \mathbf{E}$. However, except for encounters very close to the X-point the spatial separation between the peaks would be significantly larger than the primary signal discussed here. Panel (c) shows the average of the L component of the Poynting vector over the entire domain in M , $\langle S_L \rangle$, at the same time as shown in panel (b). (Averages over smaller extents exhibit

similar, albeit noisier, features.) Later in the three-dimensional simulation the LHDI drives turbulence near the X-point. Panel (d) displays $\langle S_L \rangle$ for this later time. Despite the development of the turbulence, the average structure is very similar to that at earlier times. In particular, the L -directed gradient in S_L is still present, which strongly suggests that similar physical mechanisms occur in both the two- and three-dimensional cases.

The development of turbulence in the three-dimensional case has a further effect. The resulting flows in the M - N plane twist E_N into the M direction, producing a localized $E_M \sim E_N$ that is much larger than the reconnection electric field (see Figure 10 of Price et al., 2016, for an example of this mechanism in which the source of E_N is the LHDI). As a consequence, the intense dissipation produced by $J_N E_N$ in the present 2-D simulation will also manifest in a comparable $J_M E_M$ term, an effect seen in both the three-dimensional simulation and by MMS (Burch et al., 2018).

Previous simulations of asymmetric reconnection with similar parameters have observed some of the features noted here (see, for instance, Figure 1 of Pritchett & Mozer, 2009), but they were not fully explained, perhaps due to excessive levels of computational noise. The oscillatory $\mathbf{J} \cdot \mathbf{E}$ signatures described in this work have been seen in a similar simulation, but not in simulations of MMS events with larger guide fields (see Figures 2–4 of Cassak et al., 2017). This may be due to the effects, mentioned above, of the electron diamagnetic drift. As the strength of the guide field increases (but $B_M < B_L$) the speed of the drift scales with the magnitude of B_M . For sufficiently strong fields the drift can shear the vortices seen in Figure 1b and hence may suppress the oscillatory behavior. Exploration of this idea requires further measurements and simulations of the electron diffusion region in asymmetric reconnection with guide fields of varying strength.

Acknowledgments

We gratefully acknowledge support from NASA grants NNX14AC78G, NNX16AG76G, and NNX16AF75. This research uses resources of the National Energy Research Scientific Computing Center (NERSC), a DOE Office of Science User Facility supported by the Office of Science of the U.S. Department of Energy. The simulation data are archived at NERSC and can be made available from the corresponding author by request.

References

- Bessho, N., Chen, L.-J., & Hesse, M. (2016). Electron distribution functions in the diffusion region of asymmetric magnetic reconnection. *Geophysical Research Letters*, *43*, 1828–1836. <https://doi.org/10.1002/2016GL067886>
- Burch, J. L., Ergun, R. E., Cassak, P., Webster, J. M., Torbert, R. B., Giles, B. L., et al. (2018). Localized oscillatory energy conversion in magnetopause reconnection. *Geophysical Research Letters*, *45*, 1237–245. <https://doi.org/10.1002/2017GL076809>
- Burch, J. L., Torbert, R. B., Phan, T. D., Chen, L.-J., Moore, T. E., Ergun, R. E., et al. (2016). Electron-scale measurements of magnetic reconnection in space. *Science*, *352*(6290). <https://doi.org/10.1126/science.aaf2939>
- Cassak, P. A., Genestreti, K. J., Burch, J. L., Phan, T.-D., Shay, M. A., Swisdak, M., et al. (2017). The effect of a guide field on local energy conversion during asymmetric magnetic reconnection: Particle-in-cell simulations. *Journal of Geophysical Research: Space Physics*, *122*, 11,523–11,542. <https://doi.org/10.1002/2017JA024555>
- Cassak, P. A., & Shay, M. A. (2007). Scaling of asymmetric magnetic reconnection: General theory and collisional simulations. *Physics of Plasmas*, *14*(10), 102114. <https://doi.org/10.1063/1.2795630>
- Chen, L.-J., Hesse, M., Wang, S., Bessho, N., & Daughton, W. (2016). Electron energization and structure of the diffusion region during asymmetric reconnection. *Geophysical Research Letters*, *43*, 2405–2412. <https://doi.org/10.1002/2016GL068243>
- Denton, R. E., Sonnerup, B. U. Ö., Russell, C. T., Hasegawa, H., Phan, T.-D., Strangeway, R. J., et al. (2018). Determining $L - M - N$ current sheet coordinates at the magnetopause from Magnetospheric Multiscale data. *Journal of Geophysical Research: Space Physics*, *123*, 2274–2295. <https://doi.org/10.1002/2017JA024619>
- Egedal, J., Le, A., Daughton, W., Wetherington, B., Cassak, P. A., Chen, L.-J., et al. (2016). Spacecraft observations and analytic theory of crescent-shaped electron distributions in asymmetric magnetic reconnection. *Physical Review Letters*, *117*(18), 185101. <https://doi.org/10.1103/PhysRevLett.117.185101>
- Ergun, R. E., Goodrich, K. A., Wilder, F. D., Holmes, J. C., Stawarz, J. E., Eriksson, S., et al. (2016). Magnetospheric multiscale satellites observations of parallel electric fields associated with magnetic reconnection. *Physical Review Letters*, *116*(23), 235102. <https://doi.org/10.1103/PhysRevLett.116.235102>
- Eriksson, S., Wilder, F. D., Ergun, R. E., Schwartz, S. J., Cassak, P. A., Burch, J. L., et al. (2016). Magnetospheric multiscale observations of the electron diffusion region of large guide field magnetic reconnection. *Physical Review Letters*, *117*(1), 015001. <https://doi.org/10.1103/PhysRevLett.117.015001>
- Hesse, M., Aunai, N., Sibeck, D., & Birn, J. (2014). On the electron diffusion region in planar, asymmetric systems. *Geophysical Research Letters*, *41*, 8673–8680. <https://doi.org/10.1002/2014GL061586>
- Karimabadi, H., Krauss-Varban, D., & Omid, N. (1999). Magnetic structure of the reconnection layer and core field generation in plasmoids. *Journal of Geophysical Research*, *104*(A6), 12,313–12,326. <https://doi.org/10.1029/1999JA900089>
- Le, A., Daughton, W., Chen, L.-J., & Egedal, J. (2017). Enhanced electron mixing and heating in 3-D asymmetric reconnection at the Earth's magnetopause. *Geophysical Research Letters*, *44*, 2096–2104. <https://doi.org/10.1002/2017GL072522>
- Mozer, F. S., & Pritchett, P. L. (2009). Regions associated with electron physics in asymmetric magnetic reconnection. *Geophysical Research Letters*, *36*, L07102. <https://doi.org/10.1029/2009GL037463>
- Price, L., Swisdak, M., Drake, J. F., Burch, J. L., Cassak, P. A., & Ergun, R. E. (2017). Turbulence in three-dimensional simulations of magnetopause reconnection. *Journal of Geophysical Research: Space Physics*, *122*, 11,086–11,099. <https://doi.org/10.1002/2017JA024227>
- Price, L., Swisdak, M., Drake, J. F., Cassak, P. A., Dahlin, J. T., & Ergun, R. E. (2016). The effects of turbulence on three-dimensional magnetic reconnection at the magnetopause. *Geophysical Research Letters*, *43*, 6020–6027. <https://doi.org/10.1002/2016GL069578>
- Pritchett, P. L. (2008). Collisionless magnetic reconnection in an asymmetric current sheet. *Journal of Geophysical Research*, *113*, A06210. <https://doi.org/10.1029/2007JA012930>
- Pritchett, P. L., & Mozer, F. S. (2009). The magnetic field reconnection site and dissipation region. *Physics of Plasmas*, *16*(8), 080702. <https://doi.org/10.1063/1.3206947>
- Shay, M. A., & Drake, J. F. (1998). The role of electron dissipation on the rate of collisionless magnetic reconnection. *Geophysical Research Letters*, *25*(20), 3759–3762.

- Shay, M. A., Drake, J. F., & Swisdak, M. (2007). Two-scale structure of the electron dissipation region during collisionless magnetic reconnection. *Physical Review Letters*, 99(15), 155002. <https://doi.org/10.1103/PhysRevLett.99.155002>
- Shay, M. A., Phan, T. D., Haggerty, C. C., Fujimoto, M., Drake, J. F., Malakit, K., et al. (2016). Kinetic signatures of the region surrounding the X-line in asymmetric (magnetopause) reconnection. *Geophysical Research Letters*, 43, 4145–4154. <https://doi.org/10.1002/2016GL069034>
- Sonnerup, B. U. Ö., Paschmann, G., Papamastorakis, I., Sckopke, N., Haerendel, G., Bame, S. J., et al. (1981). Evidence for magnetic field reconnection at the Earth's magnetopause. *Journal of Geophysical Research*, 86(A12), 10,049–10,067.
- Swisdak, M., Opher, M., Drake, J. F., & Alouani Bibi, F. (2010). The vector direction of the interstellar magnetic field outside the heliosphere. *Astrophysical Journal*, 710(2), 1769–1775. <https://doi.org/10.1088/0004-637X/710/2/1769>
- Swisdak, M., Rogers, B. N., Drake, J. F., & Shay, M. A. (2003). Diamagnetic suppression of component magnetic reconnection at the magnetopause. *Journal of Geophysical Research*, 108(A5), 1218. <https://doi.org/10.1029/2002JA009726>
- Tanaka, K. G., Retinò, A., Asano, Y., Fujimoto, M., Shinohara, I., Vaivads, A., et al. (2008). Effects on magnetic reconnection of a density asymmetry across the current sheet. *Annales Geophysique*, 26, 2471–2483. <https://doi.org/10.5194/angeo-26-2471-2008>
- Zeiler, A., Biskamp, D., Drake, J. F., Rogers, B. N., Shay, M. A., & Scholer, M. (2002). Three-dimensional particle simulations of collisionless magnetic reconnection. *Journal of Geophysical Research*, 107(A9), 1230. <https://doi.org/10.1029/2001JA000287>
- Zenitani, S., Hesse, M., Klimas, A., & Kuznetsova, M. (2011). New measure of the dissipation region in collisionless magnetic reconnection. *Physical Review Letters*, 106(19), 195003. <https://doi.org/10.1103/PhysRevLett.106.195003>